Available online at www.sciencedirect.com
SCIENCE DIRECT
Surface Science 600 (2006) 820–824
SURFACE SCIENCE
www.elsevier.com/locate/susc

Inelastic interactions of electrons with cylindrical interfaces

Y.H. Tu [a], C.M. Kwei [a,*], C.J. Tung [b]

[a] Department of Electronics Engineering, National Chiao Tung University, Hsinchu 300, Taiwan
[b] Department of Nuclear Science, National Tsing Hua University, Hsinchu 300, Taiwan

Received 15 July 2005; accepted for publication 1 December 2005
Available online 27 December 2005

Abstract

A theory was developed to deal with inelastic interactions for an electron moving parallel to the axis of a cylindrical structure. Formulas for the differential inverse inelastic mean free path (DIIMFP) and the total inverse inelastic mean free path (IIMFP) were derived using dielectric response theory. A sum-rule-constrained extended Drude dielectric function with spatial dispersion was applied to calculate DIIMFPs and IIMFPs for a solid wire and a cavity in solid. The calculated results showed that surface excitations occurred as the electron moved near the boundary either inside or outside the solid, whereas volume excitations arose only for electron moving inside the solid. It was found that the probability for surface excitations increases and that for volume excitations decreases for an electron moving close to the surface. Near the surface, the decrease in volume excitations is compensated by the increase in surface excitations. For a cavity in solid, the IIMFP inside the solid can be approximated by a constant value equal to the IIMFP for the infinite solid, except in the immediate vicinity of the cavity boundary.

Keywords: Electron; Cylindrical wire; Cylindrical cavity; Surface excitation; Volume excitation

1. Introduction

In recent years, technology developments permitted the production of nanometric devices with different shapes. Studies of these devices are of growing interest in surface-sensitive electron spectroscopies. The electron inelastic-interaction cross section plays an important role in the quantitative analysis of these spectra. Although the most widely studied geometry for these interactions was planar [1–5], several theoretical treatments of a cylindrical system were developed [6–8] due to improvements in the nanofabrication of cylindrical wires. Of these treatments, the single plasma resonance dielectric model was often used. Although this model is a good approximation for materials that exhibit single pole energy-loss peak, it is not so well for solids that have complex band structures.

In surface-sensitive electron spectroscopies, electron inelastic cross sections comprise mainly the contributions from volume and surface excitations. Volume and surface excitations occur when electrons travel, respectively, inside the bulk of the material and near the surface inside or outside the solid [9]. These excitations can be described using dielectric response theory. In this theory, the excitations are characterized in terms of the dielectric function of the materials. The experimental optical data and the extrapolation of these data from the optical limit to other momentum transfers are frequently used to obtain the full spectrum of the dielectric function [10–12]. Previously, an extended Drude dielectric function with spatial dispersion [13] was established with parameters determined from optical data [14]. This function was constrained by sum-rules to assure the accuracy and examined to confirm critical-point energies in the interband transitions and plasmon energies in the collective excitations. In addition, a background dielectric constant was included to account for the influence of polarized ion cores [15]. In the present work, such

* Corresponding author. Tel.: +886 3 5712121x54136; fax: +886 3 5727300.
E-mail address: cmkwei@mail.nctu.edu.tw (C.M. Kwei).

0039-6028/$ - see front matter © 2005 Elsevier B.V. All rights reserved.
doi:10.1016/j.susc.2005.12.005

a dielectric function was used to calculate the differential inverse inelastic mean free path (DIIMFP) and the total inverse inelastic mean free path (IIMFP) in a cylindrical system. These calculations were made for an electron moving parallel to the axis of the cylinder (Si wire and cavity in Si or Cu). The dependences of DIIMFP and IIMFP on electron position and energy were then analyzed. Note that all quantities are expressed in atomic units (a.u.) unless otherwise specified.

2. Theory

Fig. 1 illustrates the configuration in which an electron with velocity $\bar{v}$ moves parallel to the axis of a cylinder of radius a and dielectric function $\varepsilon_1(k,\omega)$. This cylinder is embedded in a surrounding medium of dielectric function $\varepsilon_2(k,\omega)$. At time t, the electron is at a position $\bar{x}_0 = (\rho_0, 0, vt)$ in cylindrical coordinates.

In the case that the electron moves inside the cylinder, i.e. $\rho_0 < a$, the scalar potentials can be written as [16]

$$\Phi^{(1)}(\rho,\phi,z,t) = \frac{-1}{\pi\varepsilon_1}\sum_{m=-\infty}^{\infty}\int_{-\infty}^{\infty} dk A_m e^{ik(z-vt)+im\phi} I_m(k\rho) + \frac{-1}{\pi\varepsilon_1}\sum_{m=-\infty}^{\infty}\int_{-\infty}^{\infty} dk e^{ik(z-vt)+im\phi} I_m(k\rho_<) K_m(k\rho_>) \quad (1)$$

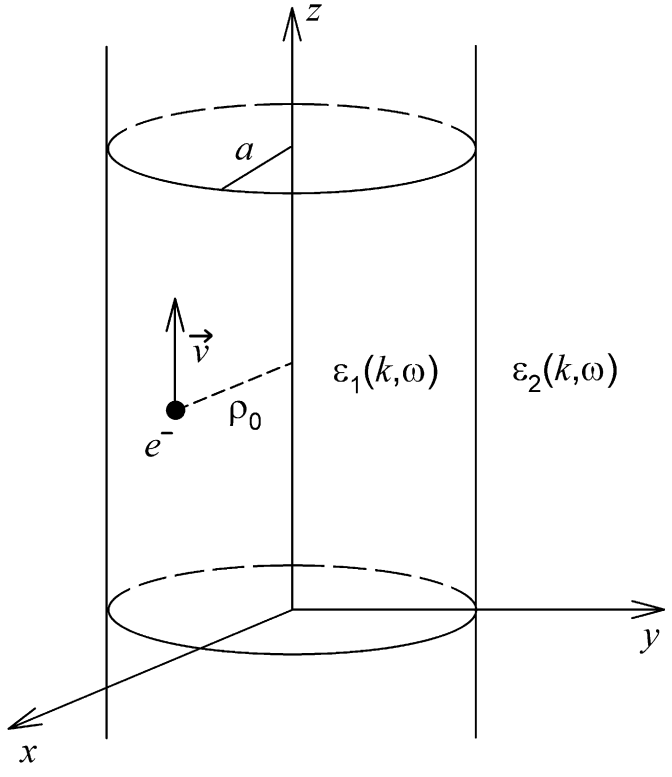

Fig. 1. A sketch of the configuration studied in the present work. An electron of velocity $\vec{v}$ moves parallel to and at a distance ρ_0 from the axis of an infinitely long cylinder of radius a. The media inside and outside the cylinder have dielectric functions $\varepsilon_1(\bar{k},\omega)$ and $\varepsilon_2(\bar{k},\omega)$, respectively.

for $\rho < a$ and

$$\Phi^{(2)}(\rho,\phi,z,t) = \frac{-1}{\pi\varepsilon_2}\sum_{m=-\infty}^{\infty}\int_{-\infty}^{\infty} dk B_m e^{ik(z-vt)+im\phi} K_m(k\rho) \quad (2)$$

for $\rho > a$, where A_m and B_m are to be determined, I_m and K_m are the modified Bessel functions, respectively, and $\rho_> = \max(\rho,\rho_0)$ and $\rho_< = \min(\rho,\rho_0)$. The Fourier transforms of these potentials are

$$\Phi^{(1)}(\rho,\phi,k,\omega) = \frac{-4\pi}{\varepsilon_1(k,\omega)}\sum_{m=-\infty}^{\infty} A_m(k,\omega) e^{im\phi} I_m(k\rho)\delta(\omega-kv) + \frac{-4\pi}{\varepsilon_1(k,\omega)}\sum_{m=-\infty}^{\infty} e^{im\phi} I_m(k\rho_<) K_m(k\rho_>)\delta(\omega-kv) \quad (3)$$

and

$$\Phi^{(2)}(\rho,\phi,k,\omega) = \frac{-4\pi}{\varepsilon_2(k,\omega)}\sum_{m=-\infty}^{\infty} B_m(k,\omega) e^{im\phi} I_m(k\rho)\delta(\omega-kv), \quad (4)$$

where δ is the delta function. Applying boundary conditions, i.e. continuity of the potential and the normal component of electric displacement at the interface $\rho = a$, one finds

$$A_m(k,\omega) = \frac{[\varepsilon_2(k,\omega)-\varepsilon_1(k,\omega)]K_m(ka)K'_m(ka)I_m(k\rho_0)}{\varepsilon_1(k,\omega)K_m(ka)I'_m(ka) - \varepsilon_2(k,\omega)I_m(ka)K'_m(ka)} \quad (5)$$

and

$$B_m(k,\omega) = \frac{\varepsilon_2(k,\omega)[K_m(ka)I'_m(ka) - I_m(ka)K'_m(ka)]I_m(k\rho_0)}{\varepsilon_1(k,\omega)K_m(ka)I'_m(ka) - \varepsilon_2(k,\omega)I_m(ka)K'_m(ka)}, \quad (6)$$

where $I'_m(x) = dI_m(x)/dx$ and $K'_m(x) = dK_m(x)/dx$. Removing the vacuum potential of an electron from the scalar potential and taking the inverse Fourier transform, the induced potential at $\rho < a$ is given by

$$\Phi^{(1)}_{\mathrm{ind}}(\rho,\phi,z,t) = \frac{-2}{\pi v}\sum_{m=-\infty}^{\infty} e^{im\phi}\int_0^E d\omega\left[I_m\left(\frac{\omega}{v}\rho\right)\times\left\{\mathrm{Re}\left[\frac{A_m\left(\frac{\omega}{v},\omega\right)}{\varepsilon_1\left(\frac{\omega}{v},\omega\right)}\right]\cos\left(\omega\left(\frac{z}{v}-t\right)\right) - \mathrm{Im}\left[\frac{A_m\left(\frac{\omega}{v},\omega\right)}{\varepsilon_1\left(\frac{\omega}{v},\omega\right)}\right]\sin\left(\omega\left(\frac{z}{v}-t\right)\right)\right\} + I_m\left(\frac{\omega}{v}\rho_<\right)K_m\left(\frac{\omega}{v}\rho_>\right)\times\left\{\mathrm{Re}\left[\frac{1}{\varepsilon_1\left(\frac{\omega}{v},\omega\right)}-1\right]\cos\left(\omega\left(\frac{z}{v}-t\right)\right) - \mathrm{Im}\left[\frac{1}{\varepsilon_1\left(\frac{\omega}{v},\omega\right)}\right]\sin\left(\omega\left(\frac{z}{v}-t\right)\right)\right\}\right]. \quad (7)$$

The stopping power, $-\frac{dW^{(1)}}{ds}$, is related to the derivative of $\Phi^{(1)}_{\mathrm{ind}}(\rho,\phi,z,t)$ at the electron position. One obtains

$$-\frac{dW^{(1)}}{ds} = \frac{-2}{\pi v^2}\sum_{m=-\infty}^{\infty}\int_0^E d\omega\omega I_m\left(\frac{\omega}{v}\rho_0\right)\left\{\mathrm{Im}\left[\frac{A_m\left(\frac{\omega}{v},\omega\right)}{\varepsilon_1\left(\frac{\omega}{v},\omega\right)}\right] + K_m\left(\frac{\omega}{v}\rho_0\right)\mathrm{Im}\left[\frac{1}{\varepsilon_1\left(\frac{\omega}{v},\omega\right)}\right]\right\}. \quad (8)$$

Note that this equation contains contributions from all relevant excitations including volume, surface and interface excitations. For an electron moving inside a cylindrical cavity, i.e. taking $\varepsilon_1 = 1$, $\varepsilon_2 = \varepsilon$ and $\omega = kv$ in Eq. (8), one obtains the formula derived by Arista et al. [7] which contains only surface excitations but no volume and interface excitations.

Since the stopping power is expressed in terms of the DIIMFP, $\mu^{(1)}$, through

$$-\frac{dW^{(1)}}{ds} = \int_0^E \omega\mu^{(1)}(E,\omega)\,d\omega, \quad (9)$$

one obtains

$$\mu^{(1)}(E,\omega) = \frac{-2}{\pi v^2}\sum_{m=-\infty}^{\infty} I_m\left(\frac{\omega}{v}\rho_0\right)\left\{\mathrm{Im}\left[\frac{A_m\left(\frac{\omega}{v},\omega\right)}{\varepsilon_1\left(\frac{\omega}{v},\omega\right)}\right] + K_m\left(\frac{\omega}{v}\rho_0\right)\mathrm{Im}\left[\frac{1}{\varepsilon_1\left(\frac{\omega}{v},\omega\right)}\right]\right\}. \quad (10)$$

A similar approach can be made for an electron moving outside the cylinder, i.e. $\rho_0 > a$. The DIIMFP is given by

$$\mu^{(2)}(E,\omega) = \frac{-2}{\pi v^2}\sum_{m=-\infty}^{\infty} K_m\left(\frac{\omega}{v}\rho_0\right)\left\{\mathrm{Im}\left[\frac{C_m\left(\frac{\omega}{v},\omega\right)}{\varepsilon_2\left(\frac{\omega}{v},\omega\right)}\right] + I_m\left(\frac{\omega}{v}\rho_0\right)\mathrm{Im}\left[\frac{1}{\varepsilon_2\left(\frac{\omega}{v},\omega\right)}\right]\right\}, \quad (11)$$

where

$$C_m(k,\omega) = \frac{[\varepsilon_2(k,\omega)-\varepsilon_1(k,\omega)]I_m(ka)I'_m(ka)K_m(k\rho_0)}{\varepsilon_1(k,\omega)K_m(ka)I'_m(ka)-\varepsilon_2(k,\omega)I_m(ka)K'_m(ka)}. \quad (12)$$

Taking $a \to \infty$ and $\varepsilon_1 = \varepsilon_2 = \varepsilon$ in Eq. (10) or $a = 0$ and $\varepsilon_1 = \varepsilon_2 = \varepsilon$ in Eq. (11), the DIIMFP in an infinite medium is obtained as

$$\mu(E,\omega) = \frac{-2}{\pi v^2}\sum_{m=-\infty}^{\infty} I_m\left(\frac{\omega}{v}\rho_0\right)K_m\left(\frac{\omega}{v}\rho_0\right)\mathrm{Im}\left[\frac{1}{\varepsilon\left(\frac{\omega}{v},\omega\right)}\right]. \quad (13)$$

The IIMFP may be calculated according to

$$\mu^{(i)}(E) = \int_0^E \mu^{(i)}(E,\omega)\,d\omega, \quad (14)$$

where $i = 1$ and 2 for an electron moving inside and outside the cylinder, respectively.

3. Results and discussion

Using Eqs. (10) and (11), the DIIMFP was calculated for an electron moving parallel to the axis of a cylindrical structure. In these calculations, a sum-rule-constrained extended Drude dielectric function with dispersion [17] was applied. Fig. 2 shows the results of this DIIMFP as a function of energy loss ω for a 500 eV electron at several distances ρ_0 from the center of a Si cylinder of radius $a = 20$ a.u. For an electron moving inside the solid, i.e. $\rho_0 < a$, the DIIMFP (upper diagram) contains two peaks corresponding to surface and volume excitations. As the electron moves closer to the cylinder surface, i.e. $\rho_0 \to a$, the volume excitation peak (~17 eV) decreases in intensity, whereas the surface excitation peak (~12 eV) increases in intensity. For an electron moving in vacuum, i.e. $\rho_0 > a$, the DIIMFP (lower diagram) is due entirely to contributions from surface excitations. The DIIMFP becomes smaller for larger electron distance from the surface. A close view of Fig. 2 reveals that the DIIMFP possesses a fine structure at low energy losses which corresponds to the band structure of Si.

Similar results for the DIIMFP of a 500 eV electron moving parallel to the axis of a cylindrical cavity in Si are plotted in Fig. 3. Again, surface excitations (~12 eV) occur for an electron moving either in the cavity (upper diagram) or in Si (lower diagram), whereas volume excitations (~17 eV) occur only for an electron in Si. For an elec-

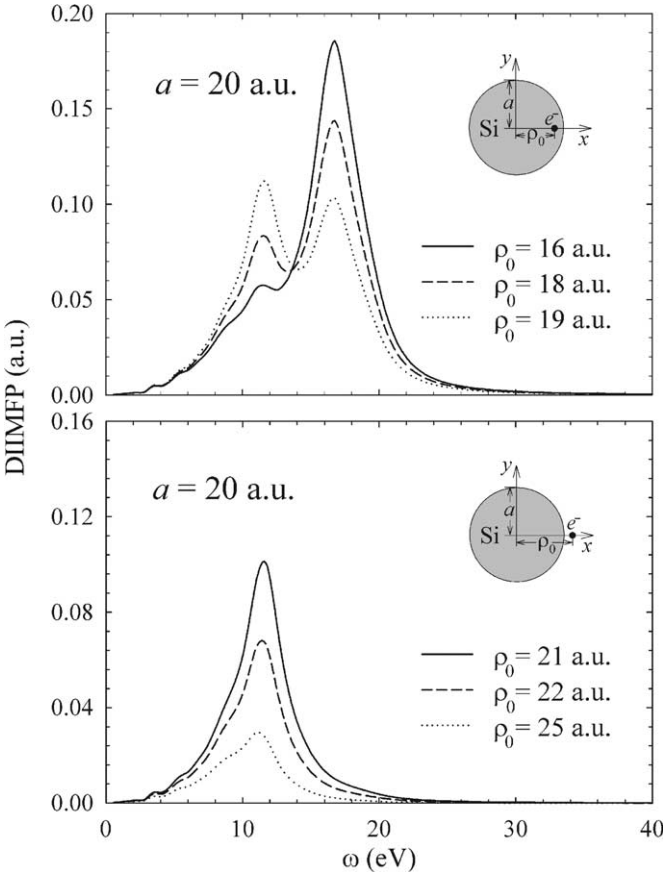

Fig. 2. Calculated DIIMFPs for a 500 eV electron moving parallel to the axis of a Si cylinder (radius $a = 20$ a.u.) in vacuum for several electron distances ρ_0 from the axis.

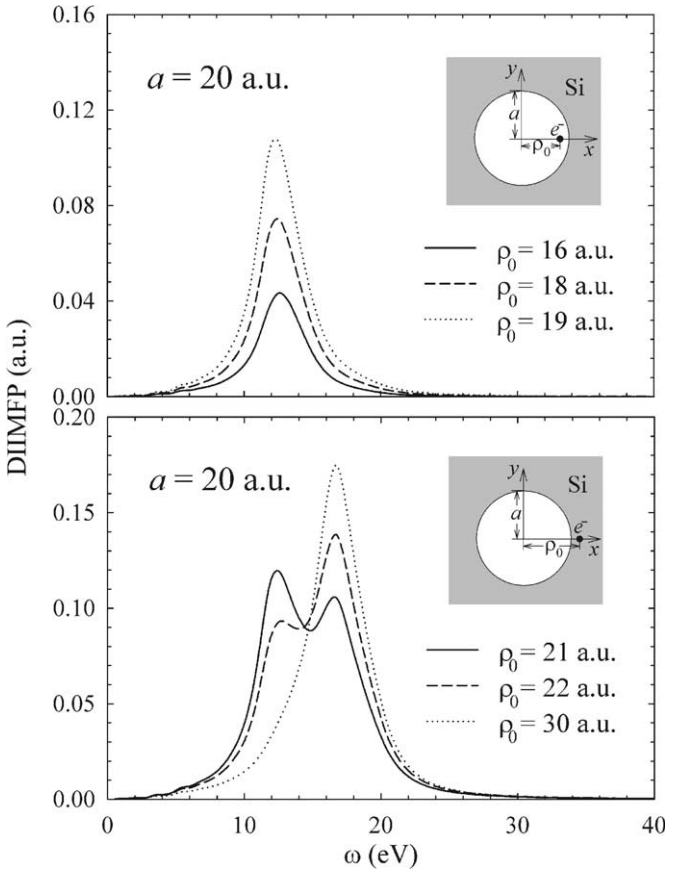

Fig. 3. Calculated DIIMFPs for a 500 eV electron moving parallel to the axis of a cylindrical cavity (radius $a = 20$ a.u.) in Si for several electron distances ρ_0 from the axis.

tron outside the cavity (lower diagram), the contributions from surface and volume excitations become smaller and larger, respectively, for increasing ρ_0. At $\rho_0 \sim 30$ a.u., the DIIMFP is due entirely to volume excitations.

Calculated DIIMFPs for a 500 eV electron moving inside a cylindrical cavity ($a = 20$ a.u.) in Si and Cu at $\rho_0 = 19$ a.u. are shown in Fig. 4. The solid curves are results using the extended Drude dielectric function. Corresponding results using the single plasma resonance dielectric function [18,19] are plotted (dotted curves) for comparison. For Si, the peak position of DIIMFPs calculated using either of those dielectric functions is nearly the same, with only a small difference in the peak magnitude. This is because Si exhibits a single pole energy-loss peak which can be described well by the electron-gas model. For Cu, although the general behavior of DIIMFP curves is similar, there is a noticeable difference between these curves. The smooth broad peak of the single plasma resonance dielectric model is the feature considering only the plasmon excitations. Whereas, a broad peak with structures is due to both plasmon and single-electron excitations of the extended Drude dielectric model. For Cu with complex band structures, the interband and intraband transitions are prominent.

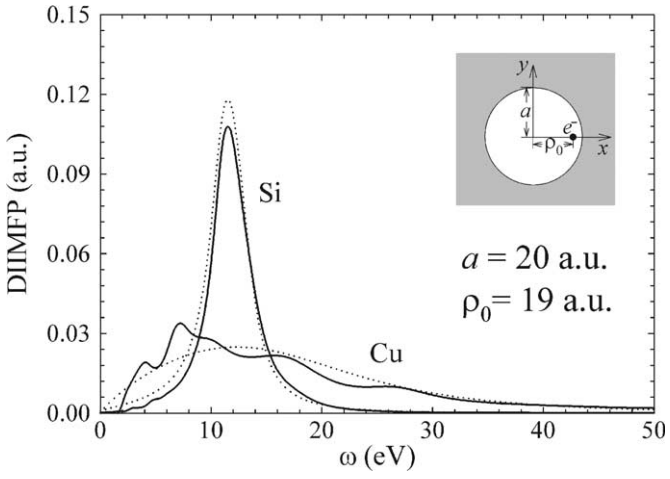

Fig. 4. DIIMFPs calculated using the extended Drude dielectric function (solid curves) and the single plasma resonance dielectric function (dotted curves) for a 500 eV electron moving parallel to and at a distance $\rho_0 = 19$ a.u. from the axis of a cylindrical cavity (radius $a = 20$ a.u.) in Si and Cu.

Fig. 5 is a plot of the DIIMFP for an electron moving outside the Si cylinder ($a = 20$ a.u.) at $\rho_0 = 21$ a.u. for several electron energies. It is seen that the DIIMFP, due only to surface excitations, decreases with increasing electron energy. The position of the surface plasmon loss peak, however, remains unchanged.

Fig. 6 shows a plot of the IIMFP for an electron moving inside ($\rho_0 < a$) or outside ($\rho_0 > a$) a cylindrical cavity in Si as a function of distance from the cavity center, ρ_0, for several electron energies. The solid and dotted curves are results calculated using the extended Drude dielectric function and the single plasma resonance dielectric function, respectively. It is seen that the IIMFP decreases with increasing electron energy for all solid and dotted curves. For a given electron energy, some discrepancies between solid and dotted curves are found. In spite of these

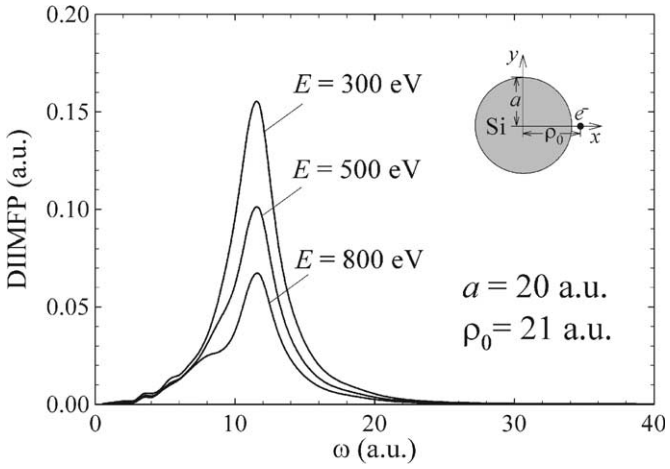

Fig. 5. Calculated DIIMFPs for an electron moving parallel to and at a distance $\rho_0 = 21$ a.u. from the axis of a Si cylinder (radius $a = 20$ a.u.) in vacuum for several electron energies.

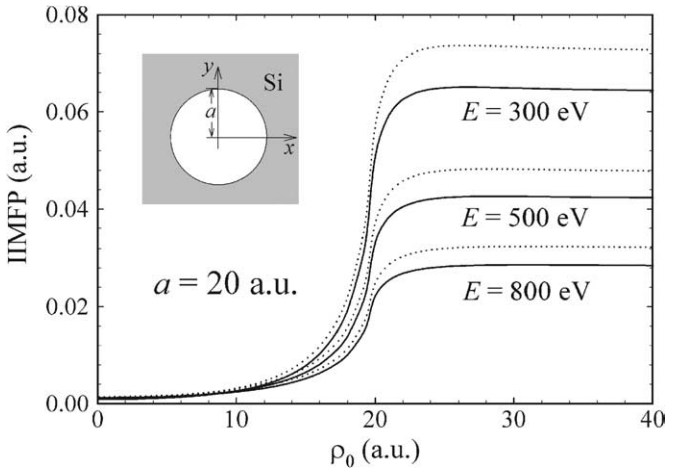

Fig. 6. IIMFPs calculated using the extended Drude dielectric function (solid curves) and the single plasma resonance dielectric function (dotted curves) for an electron moving parallel to the axis of a cylindrical cavity (radius $a = 20$ a.u.) in Si for several electron energies.

differences, the dependences of the IIMFP on electron position are all similar. In the region $\rho_0 \geqslant a$, the IIMFP has contributions from both volume and surface excitations. The contribution from surface excitations is localized to the cavity boundary and increases as $\rho_0 \to a$. On the other hand, the contribution from volume excitations is reduced near the boundary. The decrease in volume excitations is, to a good approximation, compensated by the increase in surface excitations [9]. This result makes the IIMFP spatially non-varying and approaching the value for infinite Si until the electron is closer than ~2 a.u. from the cavity boundary. The contribution from volume excitations then becomes negligibly small, and the IIMFP drops abruptly. For $\rho_0 < a$, i.e., electron inside the cavity, the IIMFP is non-zero due to surface excitations. The IIMFP decreases with decreasing ρ_0, i.e., increasing electron distance from the cavity boundary.

4. Conclusions

Analytic formulas were derived to deal with the differential and total inverse inelastic mean free paths for an electron moving parallel to the axis of a cylindrical structure based on dielectric response theory. All relevant inelastic interactions including surface and volume excitations are considered. An extended Drude dielectric function with spatial dispersion was applied to DIIMFP and IIMFP calculations for cylindrical wire and cavity. The dependences of the DIIMFP and IIMFP on the electron position and energy have been analyzed for an electron moving inside and outside the solid. These calculations showed that surface excitations are important for an electron moving near the surface. The DIIMFP and IIMFP outside the solid are entirely due to surface excitations, whereas the DIIMFP and IIMFP inside the solid are due to contributions from surface and volume excitations. The DIIMFP and IIMFP both decrease with increasing electron energy. The formulas derived in the present work can be applied to any charged particle and to a cylindrical system of arbitrary materials. Information on electron inelastic interactions with cylindrical structures is essential in the applications of electron surface spectroscopies, involving nanowires and microcapillaries.

Acknowledgement

This research was supported by the National Science Council of the Republic of China under contract no. NSC93-2215-E-009-040.

References

[1] F. Yubero, S. Tougarrd, Phys. Rev. B 46 (1992) 2486.
[2] A. Jablonski, Surf. Interface Anal. 29 (2000) 582.
[3] C.M. Kwei, Y.C. Li, Appl. Surf. Sci. 238 (2004) 151.
[4] W.S.M. Werner, Phys. Rev. B 71 (2005) 115415.
[5] C.M. Kwei, Y.H. Tu, C.J. Tung, Nucl. Instrum. Methods B 230 (2005) 125.
[6] N. Zabala, E. Ogando, A. Rivacoba, F.J. García de Abajo, Phys. Rev. B 64 (2001) 205410.
[7] N.R. Arista, M.A. Fuentes, Phys. Rev. B 63 (2001) 165401.
[8] J.L. Gervasoni, N.R. Arista, Phys. Rev. B 68 (2003) 235302.
[9] C.M. Kwei, C.Y. Wang, C.J. Tung, Surf. Interface Anal. 26 (1998) 682.
[10] R.H. Ritchie, A. Howie, Phyl. Mag. 36 (1977) 463.
[11] F. Yubero, J.M. Sanz, B. Ramskov, S. Tougaard, Phys. Rev. B 53 (1996) 9718.
[12] Z.J. Ding, J. Phys.: Condens. Matter 10 (1998) 1753.
[13] C.M. Kwei, Y.F. Chen, C.J. Tung, J.P. Wang, Surf. Sci. 293 (1993) 202.
[14] E.D. Palik (Ed.), Handbook of Optical Constants of Solids, Academic Press, New York, 1985.
[15] D.Y. Smith, E. Shiles, Phys. Rev. B 17 (1978) 4689.
[16] J.D. Jackson, Classical Electrodynamics, Wiley, New York, 1975.
[17] C.M. Kwei, S.J. Hwang, Y.C. Li, C.J. Tung, J. Appl. Phys. 93 (2003) 9130.
[18] H.J. Hinz, H. Raether, Thin Solid Films 58 (1979) 281.
[19] N.R. Arista, Phys. Rev. A 49 (1994) 1885.